JM PAPERS

A uniform current passing bodies submerged beneath an ice sheet at critical Froude numbers

Yifeng Yang[1] and Guo Xiong Wu[1]

[1]Department of Mechanical Engineering, University College London, Torrington Place, London WC1E 7JE, UK
Corresponding author: Guo Xiong Wu, g.wu@ucl.ac.uk

The problem of a uniform current interacting with bodies submerged beneath a homogeneous ice sheet is considered, based on linearised velocity potential theory for fluid and elastic thin plate theory for ice sheet. This problem is commonly solved by the boundary element method (BEM) with the Green function, which is highly effective except when the Green function becomes singular, and the direct solution of the BEM is no longer possible. However, flow behaviour, body force and ice sheet deflection near the critical Froude numbers are of major practical interest, such as in ice breaking. The present work successfully resolves this challenge. A modified boundary integral equation (BIE) is derived, which converts the singular Green function term to a far-field one and removes the singularity. The BIE is then imposed at infinity for additional unknowns in the far field. It is proved that the solution is finite and continuous at the critical Froude number $F = F_c$, where the body starts generating travelling waves, and finite but discontinuous at depth-based Froude number $F = 1^{\pm}$. Case studies are conducted for single and double circular cylinders and an elliptical cylinder with various angles of attack. A comprehensive analysis is made on the hydrodynamic forces and the generated flexural gravity wave profiles, and their physical implications are discussed. It is also concluded that the method developed in this paper is not confined to the present case but is also applicable to a variety of related problems when the BEM fails at the critical points.

Key words: wave–structure interactions, sea ice, surface gravity waves

1. Introduction

In recent years, new commercial shipping routes through the Arctic Ocean have gradually become visible (Smith & Stephenson 2013). Icebreakers are commonly

employed to ensure safe and environmentally friendly navigation for offshore operations. However, conventional icebreakers are often unsuitable for narrow channels, where limited manoeuvring space presents operational challenges, and are inefficient in thin ice conditions due to high fuel consumption and environmental impact. A promising alternative involves utilising flexural gravity waves generated by submerged vehicles (Kozin & Onishchuk 1994) or moving hovercraft on the ice sheet (Eyre 1977). To apply these methods effectively, it is crucial to understand the physical mechanisms of the hydrodynamic interactions between the moving body, flexural gravity waves and ice sheet deformation.

For loads moving on an ice sheet, Takizawa (1985) conducted an experiment on an ice-covered lake, and illustrated that the distribution of the generated flexural gravity waves in the ice sheet was related to the speed of the load. To explain this observed phenomenon, the ice sheet may be modelled as a Kirchhoff–Love plate, and the linearised velocity potential theory for the fluid may be adopted. Based on this model, Davys, Hosking & Sneyd (1985) employed the Fourier transform method and studied the three-dimensional (3-D) problem of hydroelastic waves generated by a single source moving steadily on an ice sheet. Later, Schulkes & Sneyd (1988) studied the 2-D transient problem of waves generated by moving loads. Their results showed that, for this type of problem, there are two critical Froude numbers $F = F_c$ and the depth-based $F = 1$. When $F < F_c$, there is no travelling wave to infinity and only evanescent ones; when $F_c < F < 1$, two travelling waves emerge, travelling upstream and downstream, respectively; when $F > 1$, only the upstream wave remains. Furthermore, Milinazzo, Shinbrot & Evans (1995) and Nugroho *et al.* (1999) considered the problem of flexural waves generated by prescribed point and distributed loads at the critical Froude numbers. They found that the velocity potential and ice sheet deflection for both the 2-D and 3-D problems are unbounded at $F = F_c$. In addition to a steadily moving load, Miles & Sneyd (2003) investigated the response of a floating ice sheet to a line load accelerating from rest. Their results indicated that the hydroelastic wave profile underwent a stable transition when the speed of the load passed through the critical speed $F = F_c$. More recently, Hosking & Milinazzo (2022) further extended the work to consider line loads of arbitrarily varying speed.

For bodies moving below an ice sheet, Savin & Savin (2012) simplified a 2-D circular cylinder as a dipole, and obtained an analytical solution for a dipole moving uniformly beneath a homogeneous ice sheet. Sturova (2013) further solved the 3-D problem of a sphere moving at a forward speed based on the multipole expansion procedure (Wu 1995). Li, Wu & Shi (2019) considered an equivalent problem of a uniform current interaction with a circular cylinder submerged below an ice sheet. The Green function or the velocity potential due to a single source was first derived, and then multipole expansion was adopted to construct the velocity potential. They noticed that the resistance and lift on the body experienced very rapid change when F was near F_c or 1. These were quite different from the free surface problem, where there is only one critical speed at $F = 1$ (Lighthill 1978). Later, Yang, Wu & Ren (2021) further extended the work to the 3-D ice-covered channel problem and found that the Green function is singular at an infinite number of critical speeds. A major problem when the Green function becomes singular is that the commonly used boundary element method (BEM) is no longer solvable. The behaviour of the flow corresponding to the real body then becomes unknown because the solution cannot be found. We may notice that the present case is very much different from that of a load moving on the ice sheet (Milinazzo *et al.* 1995; Nugroho *et al.* 1999), where the moving load is prescribed. Here, the potential needs to be found and its solution requires the Green function. A closely related problem is that of a body advancing at forward speed U below a free surface and oscillating with frequency ω. In the case of infinite water
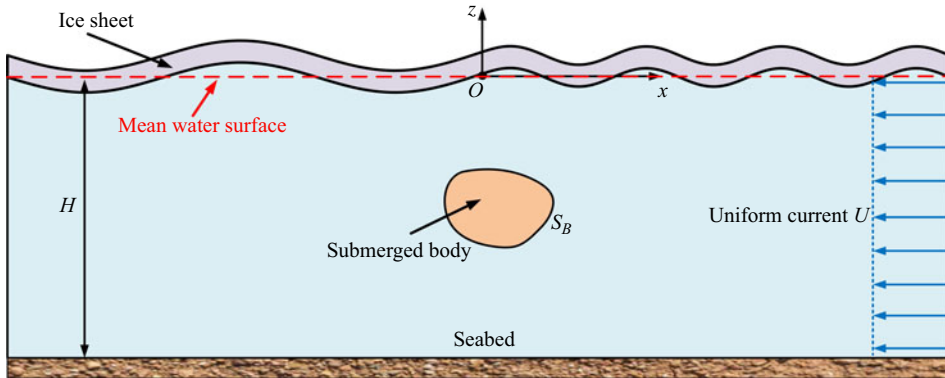
Figure 1. Sketch of the problem and the defined coordinate system.

depth, when $\tau = U\omega/g = 1/4$, where g is acceleration due to gravity, the corresponding Green function is singular and the solutions near the critical value were found to change very rapidly (Grue & Palm 1985; Wu & Eatock Taylor 1987; Wu 1991), and the problem at the critical value is not solvable. Later, Liu & Yue (1993) proved the solution for a real body of finite volume at $\tau = 1/4$. They subsequently proposed a modified boundary integral equation (BIE) for the solution at this critical point. Palm & Grue (1999) further demonstrated that the solution for a foil of zero thickness with zero volume was also finite. However, the procedure of Liu & Yue (1993) relies on the condition that an introduced parameter $\Gamma \neq 0$, which may not always be straightforward to verify in more general cases. In this paper, we propose a novel procedure to solve the problem of a uniform current passing bodies submerged beneath an ice sheet at the critical points $F = F_c$ and $F = 1$. Although the detailed derivation and results are provided only for the 2-D case, the procedure can be used in 3-D problems. In particular, a new and modified BIE is derived in which the effect of the singularity is removed. This enables us to obtain the solution at the critical Froude number directly, which has not been achieved previously, and is highly significant. Moreover, the approach here is more general and straightforward, and it can be easily applied to a wide range of related problems.

The rest of the paper is arranged as follows. The boundary value problem and the Green function are introduced in § 2. In § 3, the procedure to treat singularity and a modified BIE are proposed. In § 4, case studies and results are presented for a single and double submerged circular cylinder, as well as an ellipse with different angles of attack, followed by the conclusions in § 5.

2. The boundary value problem and the Green function

The problem of a uniform current of speed U passing a body of arbitrary shape submerged below an ice sheet sketched in figure 1 is considered. A Cartesian coordinate system $O\text{-}xz$ is defined, with the x-axis along the undisturbed water surface and against the direction of the current, and the z-axis pointing vertically upwards. The undisturbed water has depth H and its surface is covered by a homogeneous ice sheet.

The fluid with density ρ is assumed to be inviscid, incompressible and homogeneous, and its motion is irrotational. The linearised velocity potential theory is employed for the problem, as in those works mentioned above. The total velocity potential is written as

$$\Phi(x, z) = -Ux + \phi(x, z), \quad -\infty < x < +\infty, \quad -H \leqslant z \leqslant 0, \quad (2.1)$$

where ϕ denotes the disturbed velocity potential by the body, and is governed by the Laplace equation, or

$$\nabla^2 \phi = 0, \quad -\infty < x < +\infty, \quad -H \leqslant z \leqslant 0. \tag{2.2}$$

The boundary condition on the ice sheet provides (Li *et al.* 2019)

$$\left(L \frac{\partial^4}{\partial x^4} + \rho g \right) \frac{\partial \phi}{\partial z} + \rho U^2 \frac{\partial^2 \phi}{\partial x^2} = 0, \quad z = 0, \tag{2.3}$$

where L represents the flexural rigidity of the ice sheet. On the body surface S_B and the seabed, the impermeable boundary condition gives

$$\frac{\partial \phi}{\partial n} = U n_x, \quad \text{on } S_B, \tag{2.4}$$

$$\frac{\partial \phi}{\partial z} = 0, \quad z = -H, \tag{2.5}$$

where $\boldsymbol{n} = (n_x, n_z)$ represents the unit normal vector of S_B. Apart from that, the radiation condition should also be imposed at the far field, as a result of which the waves at $x = +\infty$ and $x = -\infty$ will have group velocities larger and smaller than U, respectively.

It is common that this kind of problem is solved through the BEM, in which the Green function $G(\boldsymbol{P}, \boldsymbol{Q})$, or the velocity potential at the field point $\boldsymbol{P}(x, z)$ due to a source located at $\boldsymbol{Q}(x_0, z_0)$ is essential; G satisfies all the boundary conditions above, apart from that on the body surface S_B. From Li *et al.* (2019), we have

$$G(\boldsymbol{P}, \boldsymbol{Q}) = \ln\left(\frac{r_1}{H}\right) + \ln\left(\frac{r_2}{H}\right) - 2\,\mathrm{Re}\left\{ \int_{\mathcal{L}} \frac{P(\alpha)\left[C(z, \alpha)C(z_0, \alpha)e^{i\alpha(x - x_0)} - 1\right]}{K(\alpha, U)} \,\mathrm{d}\alpha \right\}, \tag{2.6}$$

where $r_1 = \sqrt{(x - x_0)^2 + (z - z_0)^2}$, $r_2 = \sqrt{(x - x_0)^2 + (z + z_0 + 2H)^2}$ and

$$P(\alpha) = e^{-\alpha H}(L\alpha^4 + \rho g + \rho U^2 \alpha), \tag{2.7}$$

$$C(z, \alpha) = \cosh\alpha(z + H), \tag{2.8}$$

$$K(\alpha, U) = (L\alpha^4 + \rho g)\alpha \sinh(\alpha H) - \rho U^2 \alpha^2 \cosh(\alpha H). \tag{2.9}$$

The integration route $\mathcal{L}$ in (2.6) is from 0 to $+\infty$ and its path at singularities corresponding to $K(\alpha, U) = 0$ follows the procedure of Lighthill (1978). The nature of this equation has been discussed extensively by Yang, Wu & Ren (2024). When $F_c < F = U/\sqrt{gH} < 1$, where F_c denotes the critical Froude number (Davys *et al.* 1985), $K(\alpha, U) = 0$ has two positive real roots κ_{-1} and κ_0 with $\kappa_{-1} > \kappa_0$. The integration route $\mathcal{L}$ should pass under (over) the first-order poles at κ_{-1} (κ_0). The integration then can be split into the Cauchy principal integration part and the residual part. Correspondingly there will be a κ_{-1} (κ_0) wave at $x = +\infty$ ($-\infty$). When $F > 1$, κ_0 becomes a purely negative imaginary root and its wave disappears. There is only one pole at κ_{-1}, and its wave at $x = +\infty$ remains. When $F < F_c$, κ_{-1} and κ_0 become a pair of conjugate complex roots, or $\bar{\kappa}_{-1} = \kappa_0$ with $\mathrm{Re}\{\kappa_{-1}\} > 0$ and $\mathrm{Im}\{\kappa_{-1}\} > 0$. There is no singularity on $\mathcal{L}$ and no wave at infinity.

3. Solution procedure for submerged bodies at critical Froude numbers

With the help of the Green function, the differential equation for ϕ can be converted into an integral equation over the body surface (Wehausen 1973)

$$\Lambda(\boldsymbol{P})\phi(\boldsymbol{P}) = \int_{S_B}\left[\phi(\boldsymbol{Q})\frac{\partial G(\boldsymbol{P}, \boldsymbol{Q})}{\partial n_0} - G(\boldsymbol{P}, \boldsymbol{Q})\frac{\partial\phi(\boldsymbol{Q})}{\partial n_0}\right]\mathrm{d}s_0, \tag{3.1}$$

where $\Lambda(\boldsymbol{P})$ denotes the 2-D solid angle at $\boldsymbol{P}$, $\partial/\partial n_0$ represents the normal derivative at (x_0, z_0). In general, the body surface can be discretised into small elements and (3.1) can be solved numerically. However, complexity arises at a critical speed. To demonstrate the problem explicitly, we may write

$$K(\alpha, U) = (\alpha^2 - \kappa_0^2)(\alpha^2 - \kappa_{-1}^2)R_c(\alpha), \tag{3.2}$$

where $R_c(\alpha) \neq 0$ when $\alpha > 0$. Based on the discussion below (2.9), when $F \to F_c$, κ_0 and κ_{-1} merge into κ_c and $K(\alpha, U) \to (\alpha^2 - \kappa_c^2)^2 R_c(\alpha)$. In such a case, both $K(\kappa_c, U_c) = K_\alpha(\kappa_c, U_c) = 0$, where $U_c = F_c\sqrt{gH}$ and K_α denotes the derivative with respect to α. As a result, the residue at κ_c becomes infinite, or the Green function at F_c is infinite, and (3.1) becomes unsolvable. This leads to the question of whether ϕ is also infinite or exists. To answer this, we may define

$$\mathcal{F}_c(\alpha, \boldsymbol{P}, \boldsymbol{Q}) = \frac{P(\alpha)}{R_c(\alpha)}\left[C(z, \alpha)C(z_0, \alpha)e^{\mathrm{i}\alpha(x-x_0)} - 1\right], \tag{3.3}$$

where $\mathcal{F}_c(\alpha, \boldsymbol{P}, \boldsymbol{Q})$ does not contain any real pole. In such a case, G in (2.6) becomes

$$G(\boldsymbol{P}, \boldsymbol{Q}) = \ln\left(\frac{r_1}{H}\right) + \ln\left(\frac{r_2}{H}\right) - 2\,\mathrm{Re}\left\{\int_{\mathcal{L}}\frac{\mathcal{F}_c(\alpha, \boldsymbol{P}, \boldsymbol{Q})}{(\alpha^2 - \kappa_0^2)(\alpha^2 - \kappa_{-1}^2)}\,\mathrm{d}\alpha\right\}. \tag{3.4}$$

We may take out the singularities in (3.4), and write

$$\int_{\mathcal{L}}\frac{\mathcal{F}_c(\alpha, \boldsymbol{P}, \boldsymbol{Q})}{(\alpha^2 - \kappa_0^2)(\alpha^2 - \kappa_{-1}^2)}\mathrm{d}\alpha = \left(\frac{1}{\kappa_{-1}^2 - \kappa_0^2}\right)$$

$$\times \int_0^{+\infty}\left\{\left[\frac{\mathcal{F}_c(\alpha, \boldsymbol{P}, \boldsymbol{Q})}{\alpha^2 - \kappa_{-1}^2} - \frac{\mathcal{F}_c(\alpha, \boldsymbol{P}, \boldsymbol{Q})}{\alpha^2 - \kappa_0^2}\right] - \left[\frac{\mathcal{F}_c(\kappa_{-1}, \boldsymbol{P}, \boldsymbol{Q})}{\alpha^2 - \kappa_{-1}^2} - \frac{\mathcal{F}_c(\kappa_0, \boldsymbol{P}, \boldsymbol{Q})}{\alpha^2 - \kappa_0^2}\right]\right\}\mathrm{d}\alpha$$

$$+ \left(\frac{1}{\kappa_{-1}^2 - \kappa_0^2}\right)\int_{\mathcal{L}}\left[\frac{\mathcal{F}_c(\kappa_{-1}, \boldsymbol{P}, \boldsymbol{Q})}{\alpha^2 - \kappa_{-1}^2} - \frac{\mathcal{F}_c(\kappa_0, \boldsymbol{P}, \boldsymbol{Q})}{\alpha^2 - \kappa_0^2}\right]\mathrm{d}\alpha. \tag{3.5}$$

Based on the definitions of $\mathcal{L}$, κ_0 and κ_{-1}, using the residue theorem, we obtain

$$\int_{\mathcal{L}}\frac{1}{\alpha^2 - \kappa_{-1}^2}\,\mathrm{d}\alpha = \frac{\pi\mathrm{i}}{2\kappa_{-1}}, \quad \int_{\mathcal{L}}\frac{1}{\alpha^2 - \kappa_0^2}\,\mathrm{d}\alpha = -\frac{\pi\mathrm{i}}{2\kappa_0}. \tag{3.6}$$

Substituting (3.5) and (3.6) into (3.4), we have

$$G(\boldsymbol{P}, \boldsymbol{Q}) = \tilde{G}(\boldsymbol{P}, \boldsymbol{Q}) + \Psi(\boldsymbol{P}, \boldsymbol{Q}), \tag{3.7}$$

where

$$
\tilde{G}(\boldsymbol{P}, \boldsymbol{Q}) = \ln\left(\frac{r_1}{H}\right) + \ln\left(\frac{r_2}{H}\right)
$$
$$
- 2\,\mathrm{Re}\left\{\frac{1}{\kappa_{-1}^2 - \kappa_0^2} \int_0^{+\infty} \left[\begin{array}{c} \dfrac{\mathcal{F}_c(\alpha, \boldsymbol{P}, \boldsymbol{Q})}{\alpha^2 - \kappa_{-1}^2} - \dfrac{\mathcal{F}_c(\alpha, \boldsymbol{P}, \boldsymbol{Q})}{\alpha^2 - \kappa_0^2} \\ - \dfrac{\mathcal{F}_c(\kappa_{-1}, \boldsymbol{P}, \boldsymbol{Q})}{\alpha^2 - \kappa_{-1}^2} - \dfrac{\mathcal{F}_c(\kappa_0, \boldsymbol{P}, \boldsymbol{Q})}{\alpha^2 - \kappa_0^2} \end{array}\right] \mathrm{d}\alpha\right\},
$$
$$(3.8)$$

$$
\Psi(\boldsymbol{P}, \boldsymbol{Q}) = \pi\,\mathrm{Im}\left\{\frac{1}{\kappa_{-1}^2 - \kappa_0^2}\left[\frac{\mathcal{F}_c(\kappa_{-1}, \boldsymbol{P}, \boldsymbol{Q})}{\kappa_{-1}} + \frac{\mathcal{F}_c(\kappa_0, \boldsymbol{P}, \boldsymbol{Q})}{\kappa_0}\right]\right\}, \qquad (3.9)
$$

with $\mathcal{F}_c(\alpha, \boldsymbol{P}, \boldsymbol{Q})$ defined in (3.3). When $F \to F_c$, $|\kappa_{-1} - \kappa_0| \to 0$, we may apply L'Hôpital's rule to (3.8), which provides

$$
\tilde{G}(\boldsymbol{P}, \boldsymbol{Q}) = \ln\left(\frac{r_1}{H}\right) + \ln\left(\frac{r_2}{H}\right)
$$
$$
- 2\,\mathrm{Re}\left\{\mathrm{P.V.} \int_0^{+\infty} \frac{\mathcal{F}_c(\alpha, \boldsymbol{P}, \boldsymbol{Q}) - \mathcal{F}_c(\kappa_c, \boldsymbol{P}, \boldsymbol{Q})}{(\alpha^2 - \kappa_c^2)^2}\mathrm{d}\alpha\right\} + O\left(|\kappa_{-1} - \kappa_0|\right).
$$
$$(3.10)$$

Thus, $\tilde{G}$ is finite at $F = F_c$, and is consistent with the result obtained by applying the Hadamard regularisation to the integral in (3.4). By contrast, $\Psi(\boldsymbol{P}, \boldsymbol{Q})$ is singular. Besides, since $(\kappa_{-1} - \kappa_0)$ is imaginary when $F < F_c$, but real when $F_c < F < 1$, $\Psi(\boldsymbol{P}, \boldsymbol{Q})$ takes different forms when $F \to F_c + 0^{\pm}$.

We may substitute (3.7) into (3.1), which provides

$$
\Lambda(\boldsymbol{P})\phi(\boldsymbol{P}) = \int_{S_B}\left[\phi(\boldsymbol{Q})\frac{\partial\tilde{G}(\boldsymbol{P}, \boldsymbol{Q})}{\partial n_0} - \tilde{G}(\boldsymbol{P}, \boldsymbol{Q})\frac{\partial\phi(\boldsymbol{Q})}{\partial n_0}\right]\mathrm{d}s_0
$$
$$
+ \int_{S_B}\left[\phi(\boldsymbol{Q})\frac{\partial\Psi(\boldsymbol{P}, \boldsymbol{Q})}{\partial n_0} - \Psi(\boldsymbol{P}, \boldsymbol{Q})\frac{\partial\phi(\boldsymbol{Q})}{\partial n_0}\right]\mathrm{d}s_0. \qquad (3.11)
$$

The second integral in (3.11) is singular. To deal with this, we may investigate the nature of the Green function more closely. At large $|x - x_0|$, we may extend the integration route $\mathcal{L}$ in (3.4) from $\alpha \in (0, +\infty)$ to $\alpha \in (-\infty, +\infty)$. The path at the pole $-\kappa_{-1}$ $(-\kappa_0)$ is the same as that at κ_{-1} (κ_0) when it is real. When they are complex, $-\kappa_{-1}$ $(-\kappa_0)$ is in the lower (upper) half-plane. Additionally, $\overline{\kappa}_{-1} = \kappa_0$ when $F < F_c$. In such a case, the residue theorem can be used in the upper or lower half-plane, depending on the sign of $(x - x_0)$. We need to keep only the leading κ_0 and κ_{-1} terms, as well as the term due to the pole at $\alpha = 0$ in G, because other poles are on the imaginary axis (Yang *et al.* 2024) and decay far more rapidly. This provides

$$
G_{+\infty}(\boldsymbol{P}, \boldsymbol{Q}) = 2\pi\,\mathrm{Im}\left\{\frac{\mathcal{F}_c(\kappa_{-1}, \boldsymbol{P}, \boldsymbol{Q})}{\kappa_{-1}(\kappa_{-1}^2 - \kappa_0^2)}\right\} + H(F - 1) \times \pi\,\mathrm{Im}\left\{\frac{\mathcal{F}_c(-\kappa_0, \boldsymbol{P}, \boldsymbol{Q})}{\kappa_0(\kappa_{-1}^2 - \kappa_0^2)}\right\} + \mathscr{D}x,
$$
$$(3.12)$$

$$
G_{-\infty}(\boldsymbol{P}, \boldsymbol{Q}) = [2 - H(F - 1)] \times \pi\,\mathrm{Im}\left\{\frac{\mathcal{F}_c(\kappa_0, \boldsymbol{P}, \boldsymbol{Q})}{\kappa_0(\kappa_{-1}^2 - \kappa_0^2)}\right\} - \mathscr{D}x, \qquad (3.13)
$$

where the subscripts $\pm\infty$ correspond to the sign of $(x - x_0)$, $\mathscr{D}$ is a constant due to the pole at $\alpha = 0$ and $H(x)$ represents the Heaviside step function, reflecting the location of the pole at different Froude numbers. When $F < 1$, from (3.9), (3.12) and (3.13) we have

$$G_{-\infty}(\boldsymbol{P}, \boldsymbol{Q}) + G_{+\infty}(\boldsymbol{P}, \boldsymbol{Q}) = 2\Psi(\boldsymbol{P}, \boldsymbol{Q}). \tag{3.14}$$

This gives

$$\int_{S_B} \left[\phi(\boldsymbol{Q}) \frac{\partial \Psi(\boldsymbol{P}, \boldsymbol{Q})}{\partial n_0} - \Psi(\boldsymbol{P}, \boldsymbol{Q}) \frac{\partial \phi(\boldsymbol{Q})}{\partial n_0} \right] ds_0 = \pi \left[\phi_{+\infty}(\boldsymbol{P}) + \phi_{-\infty}(\boldsymbol{P}) \right], \tag{3.15}$$

where $\phi_{\pm\infty}$ represents ϕ at $x \to \pm\infty$. Applying (3.15) to (3.11), we have

$$\Lambda(\boldsymbol{P})\phi(\boldsymbol{P}) = \int_{S_B} \left[\phi(\boldsymbol{Q}) \frac{\partial \tilde{G}(\boldsymbol{P}, \boldsymbol{Q})}{\partial n_0} - \tilde{G}(\boldsymbol{P}, \boldsymbol{Q}) \frac{\partial \phi(\boldsymbol{Q})}{\partial n_0} \right] ds_0 + \pi \left[\phi_{+\infty}(\boldsymbol{P}) + \phi_{-\infty}(\boldsymbol{P}) \right]. \tag{3.16}$$

Based on the behaviour of $G_{\pm\infty}(\boldsymbol{P}, \boldsymbol{Q})$ at $F < 1$ in (3.12) and (3.13), we may write

$$\phi_{+\infty}(\boldsymbol{P}) = A_+ \mathrm{Re} \left\{ \frac{1}{\kappa_{-1}^2} \left[\frac{C(z, \kappa_{-1})}{C(0, \kappa_{-1})} e^{\mathrm{i}\kappa_{-1}x} - 1 \right] \right\} + B_+ \mathrm{Im} \left\{ \frac{1}{\kappa_{-1}} \frac{C(z, \kappa_{-1})}{C(0, \kappa_{-1})} e^{\mathrm{i}\kappa_{-1}x} \right\} + \mathscr{C}, \tag{3.17a}$$

$$\phi_{-\infty}(\boldsymbol{P}) = A_- \mathrm{Re} \left\{ \frac{1}{\kappa_0^2} \left[\frac{C(z, \kappa_0)}{C(0, \kappa_0)} e^{\mathrm{i}\kappa_0 x} - 1 \right] \right\} + B_- \mathrm{Im} \left\{ \frac{1}{\kappa_0} \frac{C(z, \kappa_0)}{C(0, \kappa_0)} e^{\mathrm{i}\kappa_0 x} \right\} - \mathscr{C}, \tag{3.17b}$$

where $A_\pm$ and $B_\pm$ are unknowns, $\mathscr{C}$ is known as the blockage constant for the free surface problem (Mei & Chen 1976). When $F \to F_c + 0^+$, both κ_{-1} and κ_0 are real and positive, and $\phi_{\pm\infty}$ are wavy functions. By contrast, when $F \to F_c + 0^-$, $\mathrm{Im}\{\kappa_{-1}\} = -\mathrm{Im}\{\kappa_0\} = \epsilon \to 0^+$, $\phi_{\pm\infty}$ decay extremely slowly with x. If $F = F_c$ is taken, $\epsilon = 0$, and they become wavy functions too. Substituting (3.17) into (3.16), and letting $F = F_c$, we obtain

$$\Lambda(\boldsymbol{P})\phi(\boldsymbol{P}) = \int_{S_B} \left[\phi(\boldsymbol{Q}) \frac{\partial \tilde{G}(\boldsymbol{P}, \boldsymbol{Q})}{\partial n_0} - \tilde{G}(\boldsymbol{P}, \boldsymbol{Q}) \frac{\partial \phi(\boldsymbol{Q})}{\partial n_0} \right] ds_0$$
$$+ \pi \left[\frac{A_+ + A_-}{\kappa_c^2} \left(\frac{C(z, \kappa_c) \cos(\kappa_c x)}{C(0, \kappa_c)} - 1 \right) + \frac{B_+ + B_-}{\kappa_c} \frac{C(z, \kappa_c) \sin(\kappa_c x)}{C(0, \kappa_c)} \right]. \tag{3.18}$$

Compared with (3.11), $\tilde{G}$ in (3.18) is finite. However, the equation has four additional unknowns, namely $A_\pm$ and $B_\pm$. To resolve that, we may let $|x| \to +\infty$ in (3.10), and invoke the theorem of residue for $\tilde{G}$. This provides

$$\lim_{|x| \to \infty} \tilde{G}(\boldsymbol{P}, \boldsymbol{Q}) = \mathrm{sgn}(x - x_0) \tilde{G}_\infty(\boldsymbol{P}, \boldsymbol{Q}) + \mathscr{D}_c |x - x_0|, \tag{3.19}$$

where $\mathrm{sgn}(x - x_0)$ is the sign function, $\mathscr{D}_c = g\pi/(gH - U_c^2)$ and

$$\tilde{G}_\infty(\boldsymbol{P}, \boldsymbol{Q}) = \frac{\pi \rho U_c^2}{2\kappa_c^2} \frac{\partial}{\partial \kappa_c} \left[\frac{\kappa_c C(z, \kappa_c) C(z_0, \kappa_c) \sin \kappa_c (x - x_0)}{R_c(\kappa_c) \sinh(\kappa_c H)} \right]. \tag{3.20}$$

In (3.19), $\tilde{G}_\infty(P, Q)$ is associated with κ_c wave terms in (3.17), and $\mathscr{D}_c|x - x_0|$ is linked to the blockage constant $\mathscr{C}$. Therefore, by letting $|x| \to +\infty$ in (3.18), it becomes

$$\pi \left[(A_+ - A_-) \frac{\cos(\kappa_c x)}{\kappa_c^2} + (B_+ - B_-) \frac{\sin(\kappa_c x)}{\kappa_c} \right] \frac{C(z, \kappa_c)}{C(0, \kappa_c)}$$
$$= \int_{S_B} \left[\phi(Q) \frac{\partial \tilde{G}_\infty(P, Q)}{\partial n_0} - \tilde{G}_\infty(P, Q) \frac{\partial \phi(Q)}{\partial n_0} \right] ds_0. \tag{3.21}$$

Substituting (3.20) into (3.21), and matching both $\sin(\kappa_c x)$ and $\cos(\kappa_c x)$ terms of the equation, we obtain

$$\int_{S_B} \left[\phi(Q) \frac{\partial \mathcal{G}_j(Q; \kappa_c)}{\partial n_0} - \mathcal{G}_j(Q; \kappa_c) \frac{\partial \phi(Q)}{\partial n_0} \right] ds_0 = 0, \quad j = 1, 2, \tag{3.22a}$$

$$A_+ - A_- = \kappa_c^2 \gamma_c \int_{S_B} \left[\phi(Q) \frac{\partial^2 \mathcal{G}_1(Q; \kappa_c)}{\partial \kappa_c \partial n_0} - \frac{\partial \mathcal{G}_1(Q; \kappa_c)}{\partial \kappa_c} \frac{\partial \phi(Q)}{\partial n_0} \right] ds_0, \tag{3.22b}$$

$$B_+ - B_- = \kappa_c \gamma_c \int_{S_B} \left[\phi(Q) \frac{\partial^2 \mathcal{G}_2(Q; \kappa_c)}{\partial \kappa_c \partial n_0} - \frac{\partial \mathcal{G}_2(Q; \kappa_c)}{\partial \kappa_c} \frac{\partial \phi(Q)}{\partial n_0} \right] ds_0, \tag{3.22c}$$

where

$$\mathcal{G}_1(Q; \kappa_c) = -\frac{C(z_0, \kappa_c)}{C(0, \kappa_c)} \sin(\kappa_c x_0), \tag{3.23a}$$

$$\mathcal{G}_2(Q; \kappa_c) = \frac{C(z_0, \kappa_c)}{C(0, \kappa_c)} \cos(\kappa_c x_0), \tag{3.23b}$$

$$\gamma_c = \frac{\rho U_c^2 \cosh^2(\kappa_c H)}{2\kappa_c R_c(\kappa_c) \sinh(\kappa_c H)}. \tag{3.23c}$$

Equation (3.22) then provides four additional equations. In such a case, the velocity potential ϕ can be solved from (3.18) and (3.22). What is important here is that there is no singular term in these equations. Also, the same equations are valid for both $F \to F_c + 0^\pm$. Hence, the solution is continuous at $F = F_c$. This then resolves the difficulty caused by the singularity of the Green function at $F = F_c$.

Apart from the critical speed at $F \to F_c$, where $(\kappa_{-1} - \kappa_0) \to 0$, there is another critical speed at $F \to 1$, where $\kappa_0 \to 0$ (Yang *et al.* 2024). In particular, when $F \to 1^-$, $\kappa_0 \to 0^+$. As can be seen from (3.8) and (3.9), the Green function is singular. Using L'Hôpital's rule in (3.3) at $\alpha = \kappa_0$, we have

$$\lim_{\kappa_0 \to 0^+} \text{Re} \{\mathcal{F}_c(\kappa_0, P, Q)\} = \frac{3\kappa_{-1}^2 \left[(z + H)^2 + (z_0 + H)^2 - (x - x_0)^2 \right]}{2H^3}. \tag{3.24}$$

Hence, (3.8) becomes

$$\tilde{G}(P, Q) = \ln \left(\frac{r_1}{H} \right) + \ln \left(\frac{r_2}{H} \right)$$
$$- 2 \, \text{Re} \left\{ P.V. \int_0^{+\infty} \left[\frac{\frac{\mathcal{F}_c(\alpha, P, Q)}{\kappa_{-1}^2 (\alpha^2 - \kappa_{-1}^2)} - \frac{\mathcal{F}_c(\alpha, P, Q)}{\kappa_{-1}^2 \alpha^2}}{+ \frac{3 \left[(z + H)^2 + (z_0 + H)^2 - (x - x_0)^2 \right]}{2H^3 \alpha^2}} \right] d\alpha \right\} + O(\kappa_0), \tag{3.25}$$

which is finite. Correspondingly (3.9) may be written as

$$\Psi(\boldsymbol{P}, \boldsymbol{Q}) = \frac{\pi}{\kappa_{-1}^2} \mathrm{Im} \left\{ \frac{\mathcal{F}_c(\kappa_0, \boldsymbol{P}, \boldsymbol{Q})}{\kappa_0} \right\} + \tilde{G}_\infty^{-1}(\boldsymbol{P}, \boldsymbol{Q}), \tag{3.26}$$

where

$$\tilde{G}_\infty^{-1}(\boldsymbol{P}, \boldsymbol{Q}) = \frac{\pi}{\kappa_{-1}^3} \mathrm{Im} \left\{ \mathcal{F}_c(\kappa_{-1}, \boldsymbol{P}, \boldsymbol{Q}) \right\}. \tag{3.27}$$

Here, $\Psi(\boldsymbol{P}, \boldsymbol{Q})$ is unbounded because of the $1/\kappa_0$ term. The singular term may also be removed using the procedure in (3.14)–(3.16). In fact, at $F = 1^-$, $\kappa_0 \to 0^+$, we may apply the theorem of residue to (3.25). Letting $|x| \to +\infty$, we obtain

$$\lim_{|x| \to \infty} \tilde{G}(\boldsymbol{P}, \boldsymbol{Q}) = \mathrm{sgn}(x - x_0) \left[\tilde{G}_\infty^{-1}(\boldsymbol{P}, \boldsymbol{Q}) + \tilde{G}_\infty^0(\boldsymbol{P}, \boldsymbol{Q}) \right] + \mathscr{D}_0 |x - x_0|, \tag{3.28}$$

where $\mathscr{D}_0 = (9\pi/5H)(1 - (5L/\rho g H^4))$, and

$$\tilde{G}_\infty^0(\boldsymbol{P}, \boldsymbol{Q}) = \frac{\pi}{2H^3}(x - x_0)^3 - \frac{3\pi}{2H^3} \left[(z + H)^2 + (z_0 + H)^2 \right](x - x_0). \tag{3.29}$$

We may further let $F = 1^-$ in (3.17b) and invoke L'Hôpital's rule. This gives

$$\phi_{-\infty}(P) = \frac{1}{2} A_- \left[(z + H)^2 - x^2 - H^2 \right] + B_- x - \mathscr{C}. \tag{3.30}$$

Substituting (3.17a) and (3.30) into (3.16), we have

$$\begin{aligned}
\Lambda(\boldsymbol{P})\phi(\boldsymbol{P}) = &\int_{S_B} \left[\phi(\boldsymbol{Q}) \frac{\partial \tilde{G}(\boldsymbol{P}, \boldsymbol{Q})}{\partial n_0} - \tilde{G}(\boldsymbol{P}, \boldsymbol{Q}) \frac{\partial \phi(\boldsymbol{Q})}{\partial n_0} \right] \mathrm{d}s_0 \\
&+ \pi \left[\frac{1}{2} A_- \left((z + H)^2 - x^2 - H^2 \right) + B_- x \right] \\
&+ \pi \left[\frac{A_+}{\kappa_{-1}^2} \left(\frac{C(z, \kappa_{-1}) \cos(\kappa_{-1} x)}{C(0, \kappa_{-1})} - 1 \right) + \frac{B_+}{\kappa_{-1}} \frac{C(z, \kappa_{-1}) \sin(\kappa_{-1} x)}{C(0, \kappa_{-1})} \right].
\end{aligned} \tag{3.31}$$

We may perform an operation similar to that in (3.18). In (3.31), letting $|x| \to +\infty$, invoking (3.28) and matching terms of $\sin(\kappa_{-1}x)$, $\cos(\kappa_{-1}x)$, $(z + H)^2 - x^2$ and x in the BIE. The following equations can be obtained:

$$A_+ = \kappa_{-1}^2 \gamma_{-1} \int_{S_B} \left[\phi(\boldsymbol{Q}) \frac{\partial \mathcal{G}_1(\boldsymbol{Q}; \kappa_{-1})}{\partial n_0} - \mathcal{G}_1(\boldsymbol{Q}; \kappa_{-1}) \frac{\partial \phi(\boldsymbol{Q})}{\partial n_0} \right] \mathrm{d}s_0, \tag{3.32a}$$

$$B_+ = \kappa_{-1} \gamma_{-1} \int_{S_B} \left[\phi(\boldsymbol{Q}) \frac{\partial \mathcal{G}_2(\boldsymbol{Q}; \kappa_{-1})}{\partial n_0} - \mathcal{G}_2(\boldsymbol{Q}; \kappa_{-1}) \frac{\partial \phi(\boldsymbol{Q})}{\partial n_0} \right] \mathrm{d}s_0, \tag{3.32b}$$

$$A_- = \int_{S_B} \left[\phi(\boldsymbol{Q}) \frac{\partial \mathcal{G}_3(\boldsymbol{Q})}{\partial n_0} - \mathcal{G}_3(\boldsymbol{Q}) \frac{\partial \phi(\boldsymbol{Q})}{\partial n_0} \right] \mathrm{d}s_0, \tag{3.32c}$$

$$B_- = \int_{S_B} \left[\phi(\boldsymbol{Q}) \frac{\partial \mathcal{G}_4(\boldsymbol{Q})}{\partial n_0} - \mathcal{G}_4(\boldsymbol{Q}) \frac{\partial \phi(\boldsymbol{Q})}{\partial n_0} \right] \mathrm{d}s_0, \tag{3.32d}$$

where $\mathcal{G}_j$ ($j = 1, 2$) are defined in (3.23a) and (3.23b), and

$$\mathcal{G}_3(\boldsymbol{Q}) = \frac{3}{H^3} x_0, \tag{3.33a}$$

$$\mathcal{G}_4(\boldsymbol{Q}) = \frac{3}{2H^3} \left[x_0^2 - (z_0 + H)^2 \right], \tag{3.33b}$$

$$\gamma_{-1} = \frac{\rho g H \cosh^2(\kappa_{-1} H)}{\kappa_{-1}^2 R_c(\kappa_{-1}) \sinh(\kappa_{-1} H)}. \tag{3.33c}$$

In such a case, $A_\pm$, $B_\pm$ and ϕ at $F = 1^-$ can be solved from (3.31) and (3.32), and the solution is finite. Moreover, if we substitute (3.32) back into (3.31), ϕ in fact can be solved directly from the BIE involving a modified Green function $G'(\boldsymbol{P}, \boldsymbol{Q})$

$$\Lambda(\boldsymbol{P})\phi(\boldsymbol{P}) = \int_{SB} \left[\phi(\boldsymbol{Q}) \frac{\partial G'(\boldsymbol{P}, \boldsymbol{Q})}{\partial n_0} - G'(\boldsymbol{P}, \boldsymbol{Q}) \frac{\partial \phi(\boldsymbol{Q})}{\partial n_0} \right] ds_0, \tag{3.34}$$

where

$$G'(\boldsymbol{P}, \boldsymbol{Q}) = \tilde{G}(\boldsymbol{P}, \boldsymbol{Q}) + \pi \gamma_{-1} \left[\mathcal{G}_2(\boldsymbol{P}; \kappa_{-1})\mathcal{G}_1(\boldsymbol{Q}; \kappa_{-1}) - \mathcal{G}_1(\boldsymbol{P}; \kappa_{-1})\mathcal{G}_2(\boldsymbol{Q}; \kappa_{-1}) \right]$$
$$+ \frac{\pi H^3}{3} \left[\mathcal{G}_3(\boldsymbol{P})\mathcal{G}_4(\boldsymbol{Q}) - \mathcal{G}_4(\boldsymbol{P})\mathcal{G}_3(\boldsymbol{Q}) \right]. \tag{3.35}$$

This removes the singularity $F = 1^-$ and involves the unknowns only on the body surface. When $F \to 1^+$, $\kappa_0 \to 0^- \times \mathrm{i}$ (Yang *et al.* 2024). We notice from (3.3) that $\mathrm{Re}\{\mathcal{F}_c(\kappa_0, \boldsymbol{P}, \boldsymbol{Q})\} \to O(\kappa_0^{-1})$, and thus (3.24) is no longer valid. To deal with that, $\mathcal{F}_c(\kappa_0, \boldsymbol{P}, \boldsymbol{Q})$ in (3.8) and (3.9) can be replaced with $[\mathcal{F}_c(\kappa_0, \boldsymbol{P}, \boldsymbol{Q}) + \mathcal{F}_c(-\kappa_0, \boldsymbol{P}, \boldsymbol{Q})]/2$. Noticing

$$\lim_{\kappa_0 \to 0} \left[\frac{\mathrm{Re}\{\mathcal{F}_c(\kappa_0, \boldsymbol{P}, \boldsymbol{Q}) + \mathcal{F}_c(-\kappa_0, \boldsymbol{P}, \boldsymbol{Q})\}}{2} \right] = \frac{3\kappa_{-1}^2 \left[(z + H)^2 + (z_0 + H)^2 - (x - x_0)^2 \right]}{2H^3}. \tag{3.36}$$

Hence, $\tilde{G}(\boldsymbol{P}, \boldsymbol{Q})$ in (3.25) is still valid. The parameter $\Psi(\boldsymbol{P}, \boldsymbol{Q})$ in (3.26) should be modified as

$$\Psi(\boldsymbol{P}, \boldsymbol{Q}) = \frac{\pi}{2\kappa_{-1}^2} \mathrm{Im} \left\{ \frac{\mathcal{F}_c(\kappa_0, \boldsymbol{P}, \boldsymbol{Q})}{\kappa_0} + \frac{\mathcal{F}_c(-\kappa_0, \boldsymbol{P}, \boldsymbol{Q})}{\kappa_0} \right\} + \tilde{G}_\infty^{-1}(\boldsymbol{P}, \boldsymbol{Q}). \tag{3.37}$$

In such a case, (3.14)–(3.16) are still satisfied. However, since κ_0 is imaginary here, $G_{\pm\infty}$ in (3.12) and (3.13) contain the decaying wave component κ_0 in both upstream and downstream regions. Based on the behaviour of G at infinity, $\phi_{\pm\infty}$ should be rewritten as

$$\phi_{+\infty}(\boldsymbol{P}) = A_+ \mathrm{Re} \left\{ \frac{1}{\kappa_{-1}^2} \left[\frac{C(z, \kappa_{-1})}{C(0, \kappa_{-1})} e^{\mathrm{i}\kappa_{-1}x} - 1 \right] \right\} + B_+ \mathrm{Im} \left\{ \frac{1}{\kappa_{-1}} \frac{C(z, \kappa_{-1})}{C(0, \kappa_{-1})} e^{\mathrm{i}\kappa_{-1}x} \right\}$$
$$+ \frac{\mathrm{i}E_+}{\kappa_0} \left[\frac{C(z, \kappa_0)}{C(0, \kappa_0)} e^{-\mathrm{i}\kappa_0 x} - 1 \right] + \mathscr{C}, \tag{3.38a}$$

$$\phi_{-\infty}(\boldsymbol{P}) = \frac{E_-}{\mathrm{i}\kappa_0} \left[\frac{C(z, \kappa_0)}{C(0, \kappa_0)} e^{\mathrm{i}\kappa_0 x} - 1 \right] - \mathscr{C}, \tag{3.38b}$$

where $E_{\pm}$ are unknowns. Letting $F = 1^+$ in (3.38a) and (3.38b), we obtain

$$\phi_{+\infty}(P) = A_+ \text{Re} \left\{ \frac{1}{\kappa_{-1}^2} \left[\frac{C(z, \kappa_{-1})}{C(0, \kappa_{-1})} e^{i\kappa_{-1}x} - 1 \right] \right\} + B_+ \text{Im} \left\{ \frac{1}{\kappa_{-1}} \frac{C(z, \kappa_{-1})}{C(0, \kappa_{-1})} e^{i\kappa_{-1}x} \right\}$$
$$+ E_+ x + \mathscr{C}, \tag{3.39a}$$

$$\phi_{-\infty}(P) = E_- x - \mathscr{C}. \tag{3.39b}$$

Following a similar procedure above, we may substitute (3.39) into (3.16). This provides

$$\Lambda(P)\phi(P) = \int_{S_B} \left[\phi(Q) \frac{\partial \tilde{G}(P, Q)}{\partial n_0} - \tilde{G}(P, Q) \frac{\partial \phi(Q)}{\partial n_0} \right] ds_0 + \pi(E_+ + E_-)x$$
$$+ \pi \left[\frac{A_+}{\kappa_{-1}^2} \left(\frac{C(z, \kappa_{-1}) \cos(\kappa_{-1}x)}{C(0, \kappa_{-1})} - 1 \right) + \frac{B_+}{\kappa_{-1}} \frac{C(z, \kappa_{-1}) \sin(\kappa_{-1}x)}{C(0, \kappa_{-1})} \right]. \tag{3.40}$$

Letting $|x| \to +\infty$ in (3.40), using (3.28), as well as matching functions $\sin(\kappa_{-1}x)$, $\cos(\kappa_{-1}x)$ and x in the BIE, (3.32a) and (3.32b) can be also obtained for A_+ and B_+. Besides, for $E_{\pm}$, we have

$$\int_{S_B} \left[\phi(Q) \frac{\partial \mathcal{G}_3(Q)}{\partial n_0} - \mathcal{G}_3(Q) \frac{\partial \phi(Q)}{\partial n_0} \right] ds_0 = 0, \tag{3.41a}$$

$$E_+ - E_- = \int_{S_B} \left[\phi(Q) \frac{\partial \mathcal{G}_4(Q)}{\partial n_0} - \mathcal{G}_4(Q) \frac{\partial \phi(Q)}{\partial n_0} \right] ds_0. \tag{3.41b}$$

Hence, the velocity potential ϕ at $F = 1^+$ can be solved from (3.32a), (3.32b), (3.40) and (3.41). These equations have no singularity. The analysis above also shows that ϕ at $F = 1^{\pm}$ is discontinuous due to the difference in the modified equations.

4. Results and discussion

In the following computation, typical values of physical parameters of the ice sheet and the fluid domain are selected as (Li *et al.* 2019)

$$\rho = 1025 \text{ kg m}^{-3}, \quad g = 9.8 \text{ m s}^{-2}, \quad L = 4.5788 \times 10^8 \text{ N m}, \quad H = 40 \text{ m}. \tag{4.1}$$

As shown in figure 2, two submerged body configurations are considered, namely, a single ellipse or two circular cylinders positioned beneath an ice sheet, for case studies. In the numerical implementation, each body surface is discretised into 128 linear elements, and equations are discretised and treated based on the procedure in Lu, He & Wu (2000), and the solution has been found to be convergent.

4.1. *Verification through a single circular cylinder submerged below an ice sheet*

Computation is first conducted for a single circular cylinder, which corresponds to a special case of figure 2(a) with dimensions $b = a = H/8$, and its centre is located at $(x_c, z_c) = (0, -2a)$. The distribution of the velocity potential ϕ on the surface of the body is shown in figure 3, where $\tan \theta = (z - z_c)/(x - x_c)$. It can be seen that the results by the modified BIE at $F = F_c$ and $F = 1^{\pm}$ are fully consistent with those by the usual BIE, or (3.1), when F is sufficiently close to these critical Froude numbers. Besides, as shown in figures 3(b) and 3(c), noticeable differences can be observed in the curves of ϕ versus θ at $F = 1^-$ and $F = 1^+$, which further verifies the proof in § 3, that ϕ is discontinuous at $F = 1$. In such a case, the solution at $F = 1$ is not unique, and any suitable linear combination
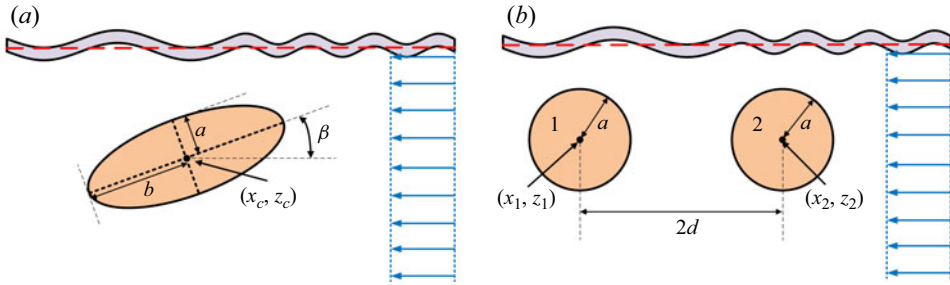
Figure 2. Sketch of the conducted case studies. (*a*) A single ellipse; (*b*) double circular cylinders.
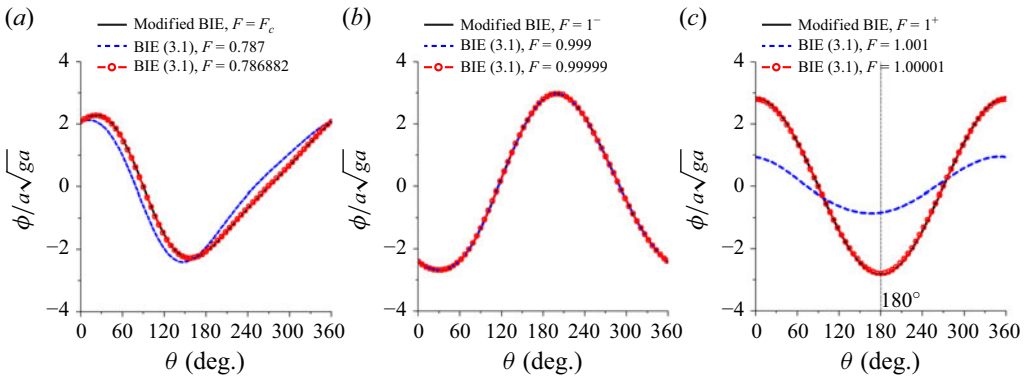

Figure 3. Velocity potential around the surface of the single circular cylinder at critical speeds: (*a*) $F \to F_c$; (*b*) $F \to 1^-$; (*c*) $F \to 1^+$; ($H = 8a$, (x_c, z_c) = (0, $-2a$), $F_c \approx 0.786882$).

of solutions at $F \to 1^-$ and $F \to 1^+$ can be a solution at $F = 1$. Furthermore, another interesting observation is that, when $F \to 1^+$, the solution of ϕ tends to Ux. This can be confirmed by substituting it into (3.32a), (3.32b), (3.40) and (3.41), and it can be verified that all these equations are satisfied. It should be noted that $\phi = Ux$ is the solution only for the case of $F = 1^+$, as it does not satisfy the far-field conditions in any other cases, including $F = 1^-$.

The resistance F_R and lift F_L on on the body can be evaluated by numerically integrating the pressure p over its surface, or

$$F_R = -\int_{S_B} p(\boldsymbol{P}) n_x \mathrm{d}s, \quad F_L = \int_{S_B} p(\boldsymbol{P}) n_z \mathrm{d}s, \tag{4.2}$$

where

$$p = -\frac{1}{2}\rho\left[\boldsymbol{\nabla}(\phi - Ux) \cdot \boldsymbol{\nabla}(\phi - Ux) - U^2\right]. \tag{4.3}$$

The minus sign in F_R means that the force is positive when it is in the direction of the incoming current. The corresponding results from BIE are shown in figure 4, where the solution based on the multipole expansion by Li *et al.* (2019), applicable for $F \neq F_c$ and $F \neq 1$, is also included for comparison and validation. Additionally, the hydrodynamic forces at $F = F_c$ and $F = 1^\pm$ are calculated using the modified BIE, with the numerical values being also presented in table 1. In figure 4(*a*), $F_R = 0$ at $F = F_c + 0^-$, which can be known from the far-field formula (Yang *et al.* 2021), since no wave exists at infinity.
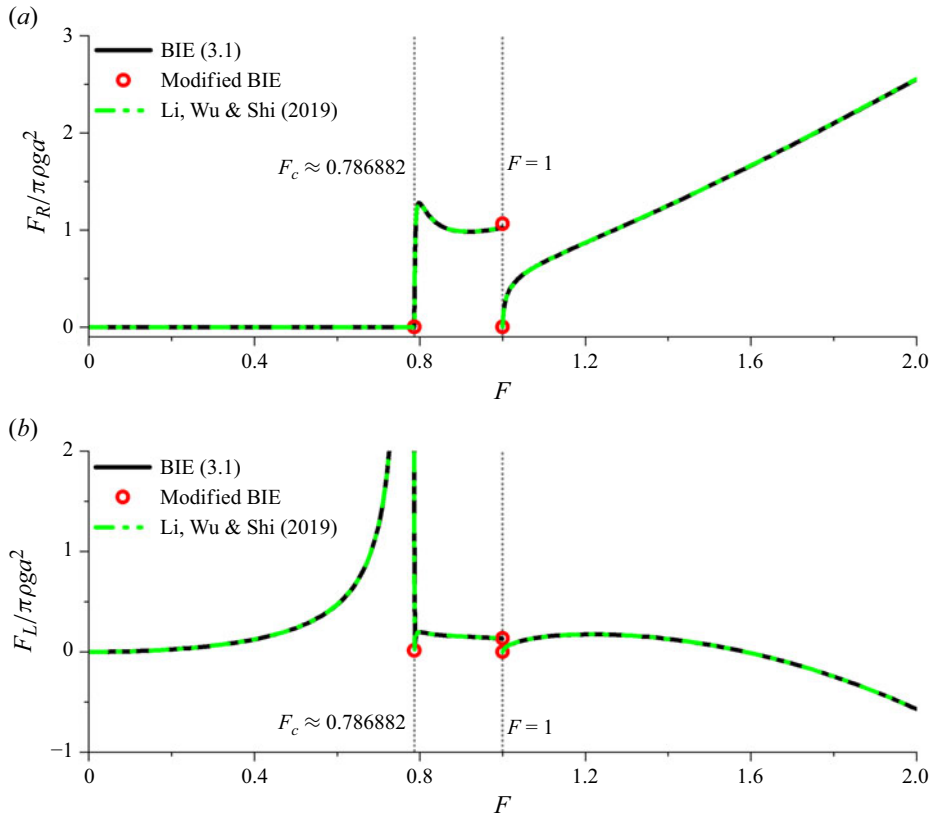
Figure 4. Resistance (*a*) and lift (*b*) on the circular cylinder versus the depth-based Froude number ($H = 8a$, $(x_c, z_c) = (0, -2a)$, $F_c \approx 0.786882$).

Hydrodynamic force	$F = F_c$	$F = 1^-$	$F = 1^+$
$F_R/\pi\rho g a^2$	0	1.0626	0
$F_L/\pi\rho g a^2$	0.0144	0.1334	0

Table 1. Resistance and lift on the circular cylinder at critical Froude numbers ($H = 8a$, $(x_c, z_c) = (0, -2a)$, $F_c \approx 0.786882$).

When F passes $F = F_c$, a rapid change occurs, followed by a peak in F_R at $F > F_c$. By contrast, in figure 4(*b*), a very large peak value of the lift F_L is observed before $F = F_c$, while at $F = F_c$, F_L is relatively small but non-zero. At $F = 1^\pm$, clear and sudden jumps in the hydrodynamic forces can be observed in both figures 4(*a*) and 4(*b*), indicating that the forces at this point are discontinuous. Besides, both F_R and F_L tend to zero as $F \to 1^+$ since $\phi \to Ux$, as discussed above.

The ice sheet deflection can be calculated from

$$\eta(x) = \frac{L}{\rho g U} \frac{\partial^4 \phi}{\partial x^3 \partial z} + \frac{U}{g} \frac{\partial \phi}{\partial x}, \quad z = 0. \tag{4.4}$$
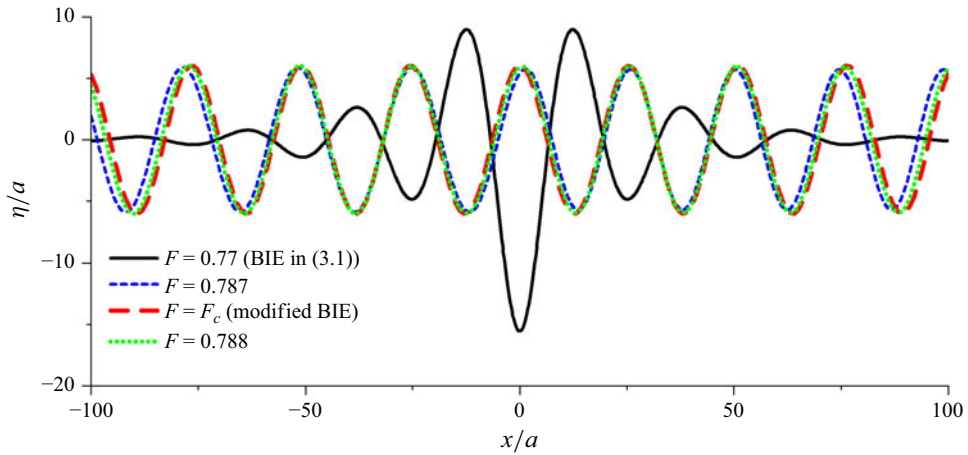
Figure 5. Ice sheet deflection η due to a circular cylinder versus x as $F \to F_c$ ($H = 8a$, $(x_c, z_c) = (0, -2a)$, $F_c \approx 0.786882$).

Figure 5 shows the ice sheet deflection $\eta(x)$ near the critical speed $F = F_c$. The maximum deflection occurs just before $F = F_c$, and forms a pronounced trough at $F = 0.77$. By contrast, $\eta(x)$ is bounded and not particularly large at $F = F_c$. This is consistent with the variation trend of the lift observed in figure 4(*b*). This behaviour implies that subcritical speeds slightly smaller than F_c may be the most efficient speeds to generate sufficient force capable of fracturing the ice sheet. The parameter $\eta(x)$ near $F = 1^{\pm}$ is presented in figure 6. The results by the conventional BIE in (3.1) gradually tend to those by the modified BIE as $F \to 1^{\pm}$. However, $\eta(x)$ tends to the result at $F = 1^-$ much more quickly than that at $F = 1^+$. In particular, a significant difference can still be observed between results at $F = 1.001$ and $F = 1^+$, even though the Froude numbers are very close. We may substitute (3.30) into (4.4). This provides $\eta(x) \to U(-A_x + B_x)/g$ as $F \to 1^-$ at $x = -\infty$, because the wavenumber downstream tends to 0. By contrast, at $F \to 1^+$, $\eta(x)$ becomes flat because ϕ tends to Ux.

4.2. *A uniform flow passing an ellipse submerged below an ice sheet*

We next analyse a submerged elliptical cylinder with aspect ratio $b/a = 2$ and its centre located at $(x_c, z_c) = (0, -2a)$, as shown in figure 2(*a*). Three angles of attack $\beta = 0°$, 15° and 30° are considered as case studies for non-circular and asymmetric bodies. The lift F_L and resistance F_R against the depth-based Froude number F are shown in figure 7, which is obtained through the usual BIE. The values of F_L and F_R at $F = F_c$ and $F = 1^{\pm}$ are computed using the modified BIE and given in table 2. In figure 7, it can be seen that the variation trends of F_L and F_R are quite similar to those of a circular cylinder shown in figure 4. For F_R in figure 7(*a*), when $F > 1$, the effect of β on the resistance is significant. At a fixed value of F, as β increases, a clear increase in F_R can be seen. For F_L in figure 7(*b*), when $F < F_c$, at a fixed value of F, F_L increases with the angle of attack β. By contrast, when $F > F_c$, the influence of β on F_L is not so obvious. Additionally, the results in table 2 further indicate that F_L is bounded and relatively small at $F = F_c$, but a very significant peak occurs just before $F = F_c$. This again suggests that an effective strategy for ice breaking by an underwater vehicle may be to operate at speeds slightly below $F = F_c$, rather than exactly at $F = F_c$.
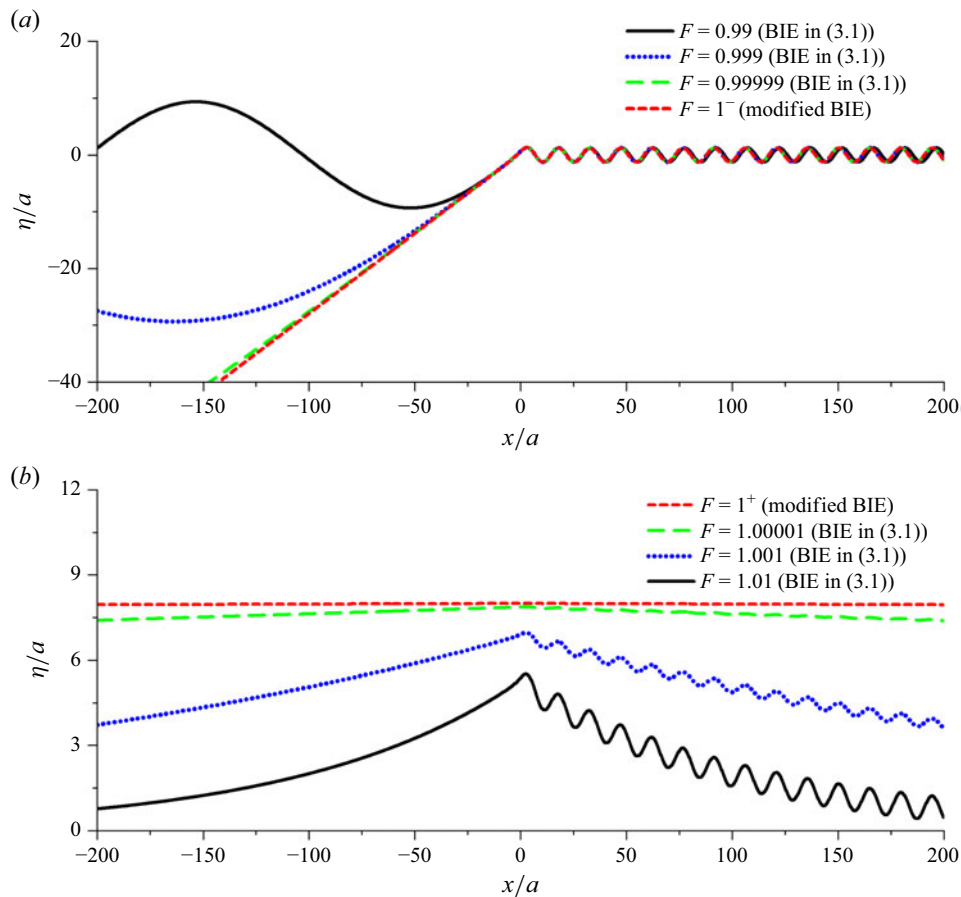
Figure 6. Ice sheet deflection η due to a circular cylinder versus x as $F \to 1$; (a) $F \to 1^-$; (b) $F \to 1^+$; ($H = 8a$, $(x_c, z_c) = (0, -2a)$, $F_c \approx 0.786882$).

Angle of attack	Hydrodynamic force	$F = F_c$	$F = 1^-$	$F = 1^+$
$\beta = 0°$	$F_R/\pi\rho g a^2$	0	1.8346	0
	$F_L/\pi\rho g a^2$	0.1037	−0.0999	0
$\beta = 15°$	$F_R/\pi\rho g a^2$	0	1.9147	0
	$F_L/\pi\rho g a^2$	0.1021	−0.1205	0
$\beta = 30°$	$F_R/\pi\rho g a^2$	0	2.5439	0
	$F_L/\pi\rho g a^2$	0.1032	0.0038	0

Table 2. Resistance and lift on an ellipse at critical Froude numbers ($H = 8a$, $b = 2a$, $(x_c, z_c) = (0, -2a)$, $F_c \approx 0.786882$).

4.3. *A uniform flow passing double circular cylinders submerged below an ice sheet*

A case study is also conducted for multiple submerged bodies, as shown in figure 2(*b*). We consider two identical circular cylinders with radius $a = H/8$, submerged at $z_1 = z_2 = -2a$, with the distance between their centres being $d = 4a$ (or $x_1 = -2a$, $x_2 = 2a$).
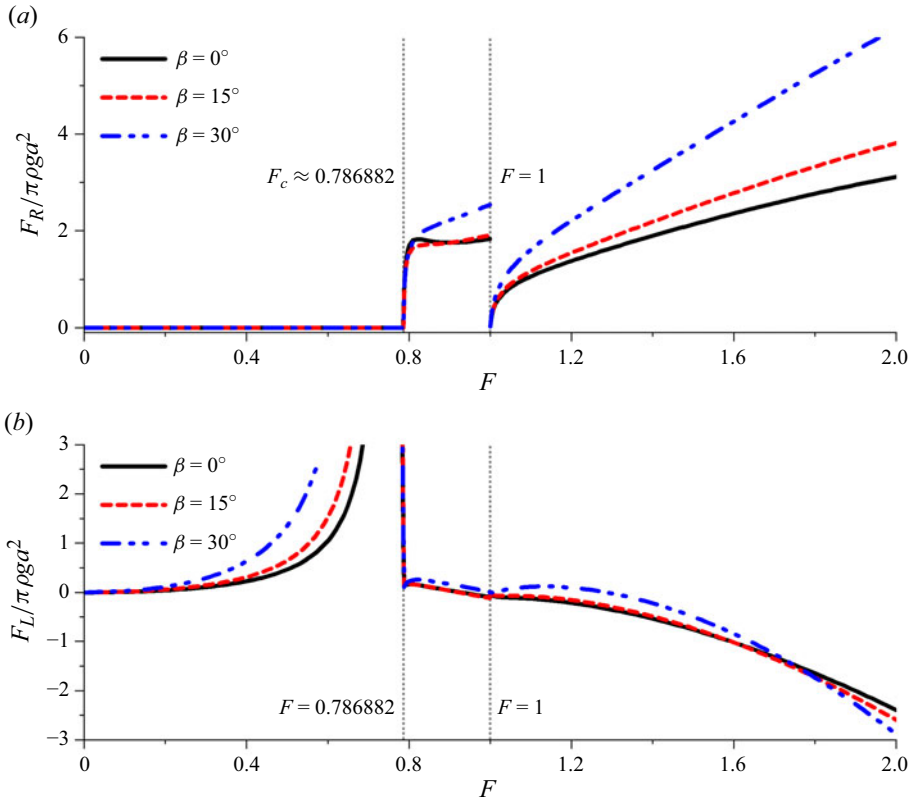
Figure 7. Resistance (*a*) and lift (*b*) on the ellipse versus the depth-based Froude number under different angles of attack ($H = 8a$, $b = 2a$, $(x_c, z_c) = (0, -2a)$, $F_c \approx 0.786882$).

The indices 1 and 2 refer to the cylinders in the downstream and upstream regions, respectively. The values of F_L and F_R versus F are shown in figure 8, and the values at critical Froude numbers are shown in table 3. When $F < F_c$, similar to the case of a single circular cylinder (Li *et al.* 2019), the profile of the flexural gravity wave should be symmetrical about the origin, and there is no wave at the far field. Hence, the total resistance should be zero. However, as shown in figure 8(*a*), the resistance on each cylinder is non-zero. When F is small, $F_R^{(1)}$ is positive and $F_R^{(2)}$ is negative, which means mutual expulsion between the two bodies. As F increases and approaches F_c, $F_R^{(1)}$ becomes negative, while $F_R^{(2)}$ becomes positive, gradually creating a strong attraction effect between the two bodies. Different from a single body, it can be seen that the resistance has a large magnitude just below the critical speed. At $F = F_c$, the magnitudes of both resistances drop to relatively small values, which can be seen in table 3. As for lift in figure 8(*b*), $F_L^{(1)} = F_L^{(2)}$ when $F < F_c$ because of symmetry. When $F_c < F < 1$, both $F_R^{(1)}$ and $F_L^{(1)}$ are positive, whereas $F_R^{(2)}$ and $F_L^{(2)}$ are always negative. At $F = 1$, clear jumps can also be found in the lifts and resistances in figure 8 and table 3. When $F > 1$, it can be seen that $F_R^{(1)}$ remains positive, while $F_R^{(2)}$ remains negative, and the attraction effect between two bodies becomes stronger as F increases within the range considered.
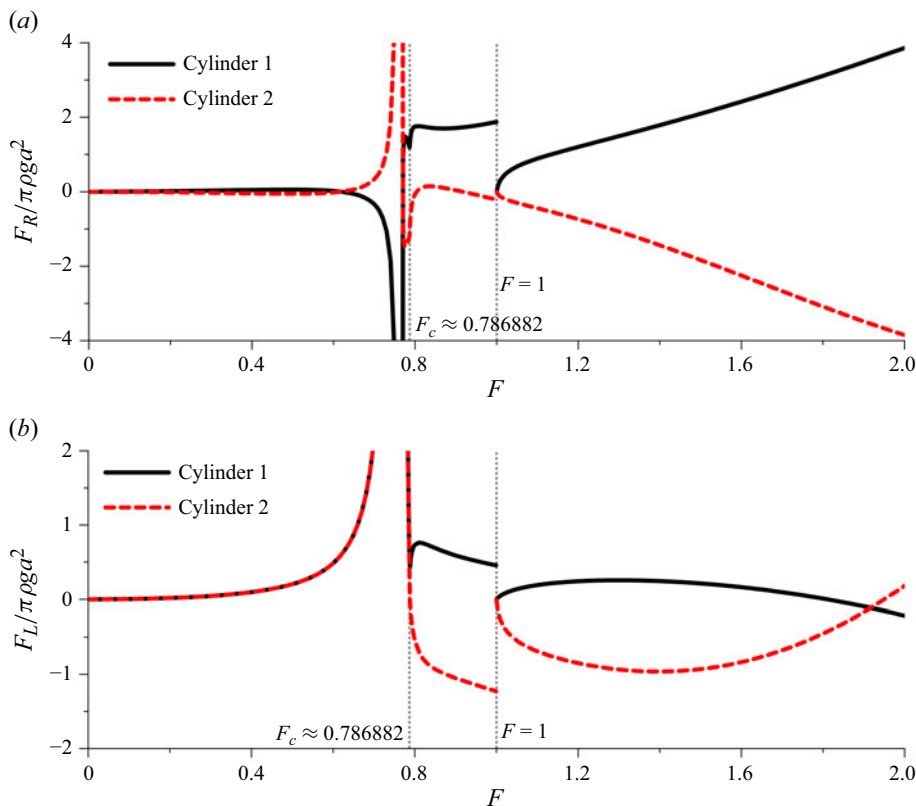
Figure 8. Resistance (*a*) and lift (*b*) on the double circular cylinders versus the depth-based Froude number ($H = 8a$, $z_1 = z_2 = -2a$, $d = 4a$, $F_c \approx 0.786882$).

Cylinder No	Hydrodynamic force	$F = F_c$	$F = 1^-$	$F = 1^+$
Cylinder 1	$F_R^{(1)}/\pi\rho g a^2$	1.1062	1.8774	0
	$F_L^{(1)}/\pi\rho g a^2$	0.2147	0.4569	0
Cylinder 2	$F_R^{(2)}/\pi\rho g a^2$	−1.1062	−0.2169	0
	$F_L^{(2)}/\pi\rho g a^2$	0.2147	−1.2284	0

Table 3. Resistance and lift on two circular cylinders at critical Froude numbers ($H = 8a$, $d = 4a$, $z_1 = z_2 = -2a$, $F_c \approx 0.786882$).

5. Conclusion

The problem of a uniform current passing bodies submerged beneath an ice sheet at the critical Froude numbers $F = F_c$ and $F = 1^\pm$ is investigated, based on the linearised velocity potential theory for the fluid and the elastic thin plate model for the ice sheet. It has been shown that, although the Green function is singular as $F \to F_c$ and $F \to 1$, the velocity potential due to a real body remains finite. Particularly, the solution is continuous at $F = F_c$, bounded but discontinuous at $F = 1^\pm$. Additionally, a modified BIE is proposed

to solve ϕ at these critical Froude numbers. The key to the success of this procedure has been to convert the singular terms in the conventional BIE to the velocity potential at the far field, thereby removing the singularity.

Various case studies are conducted to verify the mathematical proof and procedure. A single and double circular cylinder, as well as an elliptical cylinder with different angles of attack have been considered. The results are obtained through the usual BIE with F being sufficiently close to the critical Froude number and comparisons are made with results at the critical Froude number by the modified BIE. Detailed analyses are also conducted for the hydrodynamic forces on the submerged body and the generated flexural gravity waves. The following features have been observed. (i) The lift on the body is bounded and relatively small at $F = F_c$. However, when F is slightly below F_c, a large positive lift force occurs on the cylinder, which leads to a large deflection of the ice sheet. This may be used as an effective Froude number for ice breaking. (ii) When the depth-based Froude number $F = 1^+$ and $F = 1^-$, clear differences are observed in both the forces and the ice sheet deflection profiles. This further indicates that the solution at $F = 1$ may not be unique. In particular, when $F \to 1^+$, it is found that $\phi \to Ux$, which leads the hydrodynamic forces on the body to tend to 0, and the deflection profile to become flat. (iii) For a single submerged body, the resistance is zero at $F < F_c$; For multiple submerged bodies, although the total resistance is zero at $F < F_c$, the resistance on each individual body is non-zero and it can be very large when the Froude number is just below the critical one. In the case of two submerged circular cylinders, depending on F, both attraction and repulsion effects can occur between the two bodies.

The present work has successfully resolved the challenge of solving the velocity potential problem through BIE with the Green function at the critical Froude numbers. This has allowed us to obtain some detailed results and gain some insights into the physics at and near the critical Froude number. What is more significant is that the solution procedure developed in this work is not just confined to the current problem, but can also be used in a wide range of related problems, for example, the singular problem in Liu & Yue (1993), the singular problem of fluid and structure interaction at critical Froude numbers or natural frequencies in an ice-covered channel Yang *et al.* (2021, 2022) and also a uniform current interaction with a 3-D body in unbounded ocean.

Declaration of interests. The authors report no conflict of interest.

REFERENCES

DAVYS, J.W., HOSKING, R.J. & SNEYD, A.D. 1985 Waves due to a steadily moving source on a floating ice plate. *J. Fluid Mech.* **158**, 269–287.

EYRE, D. 1977 The flexural motions of a floating ice sheet induced by moving vehicles. *J. Glaciol.* **19** (81), 555–570.

GRUE, J. & PALM, E. 1985 Wave radiation and wave diffraction from a submerged body in a uniform current. *J. Fluid Mech.* **151**, 257–278.

HOSKING, R.J. & MILINAZZO, F. 2022 Two-dimensional response of a floating ice plate to a line load moving at variable speed. *J. Fluid Mech.* **938**, A2.

KOZIN, V.M. & ONISHCHUK, A.V. 1994 Model investigations of wave formation in solid ice cover from the motion of a submarine. *J. Appl. Mech. Tech. Phys.* **35** (2), 235–238.

LI, Z.F., WU, G.X. & SHI, Y.Y. 2019 Interaction of uniform current with a circular cylinder submerged below an ice sheet. *Appl. Ocean Res.* **86**, 310–319.

LIGHTHILL, J. 1978 *Waves in Fluids*. Cambridge University Press.

LIU, Y.M. & YUE, D.K.P. 1993 On the solution near the critical frequency for an oscillating and translating body in or near a free surface. *J. Fluid Mech.* **254**, 251–266.

LU, C.H., HE, Y.S. & WU, G.X. 2000 Coupled analysis of nonlinear interaction between fluid and structure during impact. *J. Fluids Struct.* **14** (1), 127–146.

MEI, C.C. & CHEN, H.S. 1976 A hybrid element method for steady linearized free-surface flows. *Intl J. Numer. Meth. Engng* **10** (5), 1153–1175.

MILES, J. & SNEYD, A.D. 2003 The response of a floating ice sheet to an accelerating line load. *J. Fluid Mech.* **497**, 435–439.

MILINAZZO, F., SHINBROT, M. & EVANS, N.W. 1995 A mathematical analysis of the steady response of floating ice to the uniform motion of a rectangular load. *J. Fluid Mech.* **287**, 173–197.

NUGROHO, W.S., WANG, K., HOSKING, R. & MILINAZZO, F. 1999 Time-dependent response of a floating flexible plate to an impulsively started steadily moving load. *J. Fluid Mech.* **381**, 337–355.

PALM, E. & GRUE, J. 1999 On the wave field due to a moving body performing oscillations in the vicinity of the critical frequency. *J. Engng Maths* **35** (1), 219–232.

SAVIN, A. & SAVIN, A. 2012 Ice cover perturbation by a dipole in motion within a liquid. *Fluid Dyn.* **47** (1), 139–146.

SCHULKES, R.M.S.M. & SNEYD, A.D. 1988 Time-dependent response of floating ice to a steadily moving load. *J. Fluid Mech.* **186**, 25–46.

SMITH, L.C. & STEPHENSON, S.R. 2013 New Trans-Arctic shipping routes navigable by midcentury. *Proc. Natl Acad. Sci. USA* **110** (13), E1191–E1195.

STUROVA, I.V. 2013 Unsteady three-dimensional sources in deep water with an elastic cover and their applications. *J. Fluid Mech.* **730**, 392–418.

TAKIZAWA, T. 1985 Deflection of a floating sea ice sheet induced by a moving load. *Cold Reg. Sci. Technol.* **11** (2), 171–180.

WEHAUSEN, J.V. 1973 The wave resistance of ships. *Adv. Appl. Mech.* **13**, 93–245.

WU, G.X. 1991 Hydrodynamic forces on a submerged cylinder advancing in water waves of finite depth. *J. Fluid Mech.* **224**, 645–659.

WU, G.X. 1995 Radiation and diffraction by a submerged sphere advancing in water waves of finite depth. *Proc. R. Soc. Lond. A* **448** (1932), 29–54.

WU, G.X. & EATOCK TAYLOR, R. 1987 Hydrodynamic forces on submerged oscillating cylinders at forward speed. *Proc. R. Soc. Lond. A* **414** (1847), 149–170.

YANG, Y.F., WU, G.X. & REN, K. 2021 Three-dimensional interaction between uniform current and a submerged horizontal cylinder in an ice-covered channel. *J. Fluid Mech.* **928**, A4.

YANG, Y.F., WU, G.X. & REN, K. 2022 Hydroelastic wave diffraction by a vertical circular cylinder standing in a channel with an ice cover. *J. Fluid Mech.* **941**, A13.

YANG, Y.F., WU, G.X. & REN, K. 2024 Interaction between a uniform current and a submerged cylinder in a marginal ice zone. *J. Fluid Mech.* **984**, A50.